AIAA JOURNAL
Vol. 39, No. 12, December 2001

Numerical Analysis of Reducing Driver Gas Contamination in Impulse Shock Tunnels

Y. Burtschell,* M. Cardoso,† and D. E. Zeitoun‡
Universite de Provence–Technopole de Chateau Gombert, 13453 Marseille Cedex 13, France

A numerical analysis was carried out to study the interaction of the reflected shock with incident boundary layer and contact surface in reflected shock tunnels and the driver gas contamination of the hot flow, in tailored conditions. Navier–Stokes equations were solved with a multiblock finite volume method in a shock tube and a nozzle. Different suction devices, such as a corner slit, a corner slit prolongated by a sleeve, and a conical ring, were tested for their capability of delaying this contamination effect. The results show that the driver gas passes through a bifurcated shock foot as a jet and causes premature contamination of the driven gas. They also show why the suction induced by a corner slit is inefficient for delaying the contamination. Located just behind the bifurcated shock foot after the shock/interface interaction, the sleeve device captures driver gas upstream and leads to an improvement in the driver gas arrival time by a factor of 1.8. Finally, based on the present numerical investigation, a new conical ring device is proposed, with a horizontal and vertical suction, which further increases this factor to 2.5.

I. Introduction

REFLECTED shock-tunnel facilities are generally used for obtaining high-enthalpy stagnation flows. These facilities end with super- or hypersonic nozzles and a test chamber, which contains the model to be studied. The flow test time, during which experiments can be made, strongly depends on the time homogeneity of the hot flow reservoir conditions.[1] These flow conditions are obtained after shock wave reflection at the end of the tube and driver/driven gas interface tailoring. The theoretical test time can be defined as the necessary time for the hot gas mass to pass through the nozzle until the arrival of cold driver gas.

Several effects contribute to reducing this test time, such as the wall boundary layer increasing behind the moving incident shock wave,[2–4] the transient flow in the nozzle, and the reflected shock interaction with the incident boundary layer.[5] This interaction yields a bifurcation at the foot of this reflected shock. After shock/interface meeting, the driver gas passes through this bifurcation region and penetrates this interface as a jet along the tube wall to contaminate the hot test gas. Mark,[5] Davies and Wilson,[6] and Stalker and Crane[7] have successively studied this contamination effect. More recently, the reflected shock/boundary-layer interaction has been numerically described by several authors, such as Nishida and Lee,[8] Chue and Itoh,[9] and Wilson et al.[10]

From an experimental point of view and up to the past few years, experimental devices did not exist to measure this contamination in high-enthalpy reflected shock tunnels to validate these existing theories or computational results. In 1993, Slade et al.[11] studied driver gas detection by quadrupole mass spectrometry. In 1995, Paull and King[12] proposed a simple detector consisting of a square duct and a wedge. The shock angle produced by the wedge is modified by the driver gas composition and allows a chocked flow and a pressure increase to be obtained. Recently, Sudani and Hornung[13] improved this device by adding a wedge in the duct, and a flat plate to the outer wall of the square duct, and both are installed at a relatively high angle of attack to the freestream. From their experimental results in the T5 Hypervelocity Shock Tunnel, they validate the Davies and Wilson[6] theory for the available test time and show that it is possible to increase it slightly by using undertailored conditions. Nevertheless, the contamination problem is present, and Sudani and Hornung[13] claim that "increased test time is required, especially at high enthalpy flows and methods for delaying contamination are under development."

A means of diminishing the incident boundary-layer development is sucking the driver gas jet passing through the bifurcation region at the foot of the reflected shock. The most simple and well-known idea is to create a suction through the wall tube to delay the contamination of the test gas. However, the main difficulty is to know how and where to locate this suction to have a strong effect.

Dumitrescu[14] proposed locating this suction at the corner of the end wall of the shock tube. He experimentally showed a decrease in tangential velocity and an increase in pressure plateau at the end wall of the tube. These experiments were made without the starting process in the nozzle. Sudani et al.[15] used the same experimental device in their T5 shock tunnel and concluded that this device is inefficient to reduce the contamination of the test gas. The same conclusion was obtained by Chue and Dumitrescu[16] and Cardoso et al.[17] numerically. This conclusion results because the driver gas passing through the bifurcation region is deflected toward the nozzle entrance before it reaches the end of the tube.

The idea of creating this suction upstream, by using a sleeve for capturing the driver gas before its propagation in the test gas, has been proposed and numerically studied by Cardoso et al.[17] and experimentally by Sudani et al.[15]

The aim of the present paper is to study the complete description of reflected flow at the end of tube numerically from the starting up to steady flow in the nozzle, as well as its contamination by driver gas with and without different devices for wall suction. The complete unsteady two-dimensional axisymmetric Navier–Stokes equations of an He/N_2 mixture flow are solved by the multiblock finite volume method. The inviscid fluxes on cell interfaces are computed by an approximate Rieman solver based on a MUSCL approach with second-order total variation diminishing (TVD) extension. (This numerical code is called the CARBUR code.[18]) The numerical results obtained from an incident Mach number equal to 6 are compared and discussed. An efficient solution has been found to reduce the contamination effect strongly, which leads to a dramatic improvement in the useful test time.

Received 2 November 1998; revision received 29 August 2000; accepted for publication 16 May 2001.

*Maitre de Conferences, Laboratoire Institut Universitaire Systemes Thermiques Industriels (Centre National de la Recherche Scientifique 6595), Departement Milieux Hors d'Equilibre, 5 rue Enrico Fermi.

†Ph.D. Student, Laboratoire Institut Universitaire Systemes Thermiques Industriels (Centre National de la Recherche Scientifique 6595), Departement Milieux Hors d'Equilibre, 5 rue Enrico Fermi.

‡Professor, Fluid Dynamics, Laboratoire Institut Universitaire Systemes Thermiques Industriels (Centre National de la Recherche Scientifique 6595), and Head, Departement Milieux Hors d'Equilibre, 5 rue Enrico Fermi. Senior Member AIAA.

Table 1 Initial conditions in the reflected shock tunnel

Variable	Driver gas, He	Driven gas, N_2	Nozzle
Pressure, MPa	17.2	0.0552	0.0001
Temperature, K	853	300	300

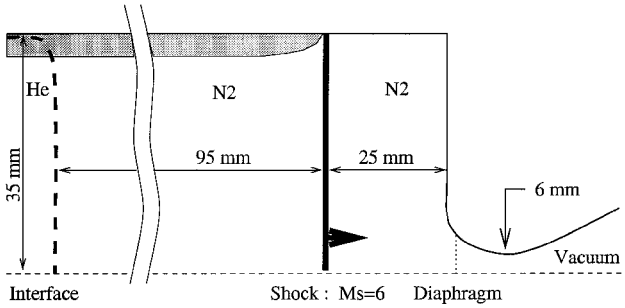

Fig. 1 Schematic of the reflected shock tunnel.

II. Position of the Problem

To describe the contamination processes of the hot test gas due to the reflected shock and contact surface interaction numerically, a shock tube reduced in its length (about a factor 10) with its exact diameter has been chosen. The influence of this shortening effect on the test time will be discussed in Sec. IV. These low-pressure chamber dimensions are chosen equal to 0.6 m in length and 0.07 m in diameter. The nozzle length is 3.5 cm, and its throat diameter is 1.2 cm. These diameters correspond to those of the Marseille free piston shock tube facility (TCM2).[19] These dimensions allow a detailed description of the unsteady flowfield to be obtained with a lower CPU time and a finer mesh in the computational domain. Figure 1 shows a schematic view of the reflected shock tunnel. The driver/driven gases are, respectively, He/N_2 with initial conditions given in Table 1. In Table 1, the initial conditions in the nozzle are also reported.

These conditions lead to an incident Mach number equal to 6.02 with an instantaneous opening of the diaphragm and N_2 frozen flow assumptions. The reservoir conditions, after reflection of the shock wave at the end of the tube and with tailored conditions, are equal to 16.3 MPa for the pressure and to 5074 K for the temperature. They correspond to a specific reservoir enthalpy of 5.2 MJ/kg. Now, if sonic conditions are assumed at the nozzle throat, the computed ideal mass flow rate is equal to 1.058 kg/s, which gives an ideal drainage time of 1.39 ms through the nozzle.

III. Governing Equations and Numerical Method

The unsteady compressible laminar shock tube and nozzle flows are governed by either Euler equations for inviscid flow conditions or Navier–Stokes equations in the viscous flow case. These equations can be written as follows:

$$\frac{\partial U}{\partial t} + \nabla \cdot \boldsymbol{F}(\boldsymbol{U}) = 0$$

where $\boldsymbol{U} = (\rho Y_{He}, \rho Y_{N_2}, \rho u, \rho v, \rho e)^t$ is the conserved vector of flow variables and $\boldsymbol{F} = \boldsymbol{F}_e + \boldsymbol{F}_v$ is the sum of convective $\boldsymbol{F}_e$ and viscous $\boldsymbol{F}_v$ flux vectors. Assuming a perfect gas, the thermodynamic variables are related by the state equation

$$P = (\gamma - 1)\rho\varepsilon$$

In the preceding equations, ρ is the density, Y is the species mass fractions, u and v are the components of the velocity, and e and ε are the total and specific energy per unit mass.

A finite difference approximation of these conservation laws, in a two-dimensional axisymmetric system, is formulated as an explicit multiblock finite volume method on a structured grid. This grid is made of rectangular or quadrilateral cells. On each cell *(i, j)*, the finite difference approximation of these equations can be written as follows:

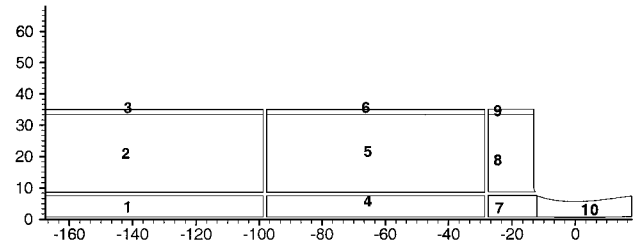

Fig. 2 Multiblock computational domain.

$$\frac{\partial U_{i,j}}{\partial t} + \frac{1}{A_{i,j} r_{i,j}^{\alpha}} \sum_{k=1}^{4} \boldsymbol{F}_k \boldsymbol{N}_k = \alpha H_{i,j}$$

where $\alpha = 1$ for a two-dimensional axisymmetric coordinate system ($\alpha = 0$ for planar two-dimensions), $A_{i,j}$ is the area of the cell *(i, j)*, $\boldsymbol{N}_k$ is the outward normal vector on each side of the cell, $H_{i,j}$ is the axisymmetric source term, and $r_{i,j}$ is the radius of the cell-center position.

The convective flux terms are discretized through a second-order TVD extension based on a MUSCL approach and an approximate Rieman solver HLLEMR proposed in Ref. 20. The viscous terms are classically discretized by a second-order central difference approximation. A time predictor–corrector algorithm is used to obtain second-order time accuracy. Concerning the boundary conditions, on the shock tube and nozzle walls, no-slip conditions for the velocity components and adiabatic wall conditions are imposed; on the centerline, symmetry boundary conditions are implemented. A detailed description of this numerical method (CARBUR) may be found in Refs. 18 and 20. The computational domain is divided into 6–10 blocks, as a function of the computational domain (shown in Fig. 2) with a total of 10,000 mesh points. The y mesh distribution is stretched near the wall with a minimum mesh size equal to 2×10^{-5} m. This value leads to a first nondimensional cell center of the wall $y^+ = 5$. Others values, such as 4×10^{-5} and 1×10^{-5} m, will be tested to study the grid dependence. In the same way, the x mesh distribution is also nonuniform with a minimum mesh size of 1×10^{-4} m. The time step is classically determined by explicit stability criteria and the Courant–Friedrichs–Lewy (CFL) number used in all computations presented is equal to 0.5.

IV. Numerical Results and Discussion

All of the computations are run in the shock tube for 0.268 ms starting from the He/N_2 diaphragm rupture. This is to locate the shock wave at 2.5 cm before the end of the tube with a separation distance between the shock and the contact surface equal to 9.5 cm (Fig. 1). This computed plane is taken as the initial condition. The shock wave arrives at the end of tube at time equal to 0.280 ms.

A. Euler Solutions

This computation is only made to test the capability of the numerical code to reproduce the tailoring of the contact surface and to compute the test time in the nozzle for an inviscid flow. The time evolution of N_2 mass fractions is shown in Fig. 3. It can be seen that the reflected shock interacts with the contact surface at a time equal to 0.321 ms (Fig. 3a). From this time, the contact surface is tailored. In addition, the unsteady flow starting in the nozzle leads to a complex wave system in the nozzle entrance, which speeds up the flow in the stagnation region near the end wall. This induces a deformation of the contact surface (Figs. 3b–3d), and its upper part moves with the flow (Figs. 3e and 3f). A rollup effect is established in the hot flow reservoir. Thus, the contact surface enters the nozzle, and a little part of the hot flow is trapped by this rollup effect. To measure this contamination, 5% of the He level has been chosen to characterize the upstream front of the contact surface. This value corresponds to the existing detector sensitivity.[13] The arrival time of this contact surface in the nozzle, after the reflected shock wave, can be considered as the inviscid test time, and it is equal to 0.87 ms. This value is 63% of the ideal drainage time (1.39 ms). The discrepancy is partially due to the unsteady flow effects and also to the

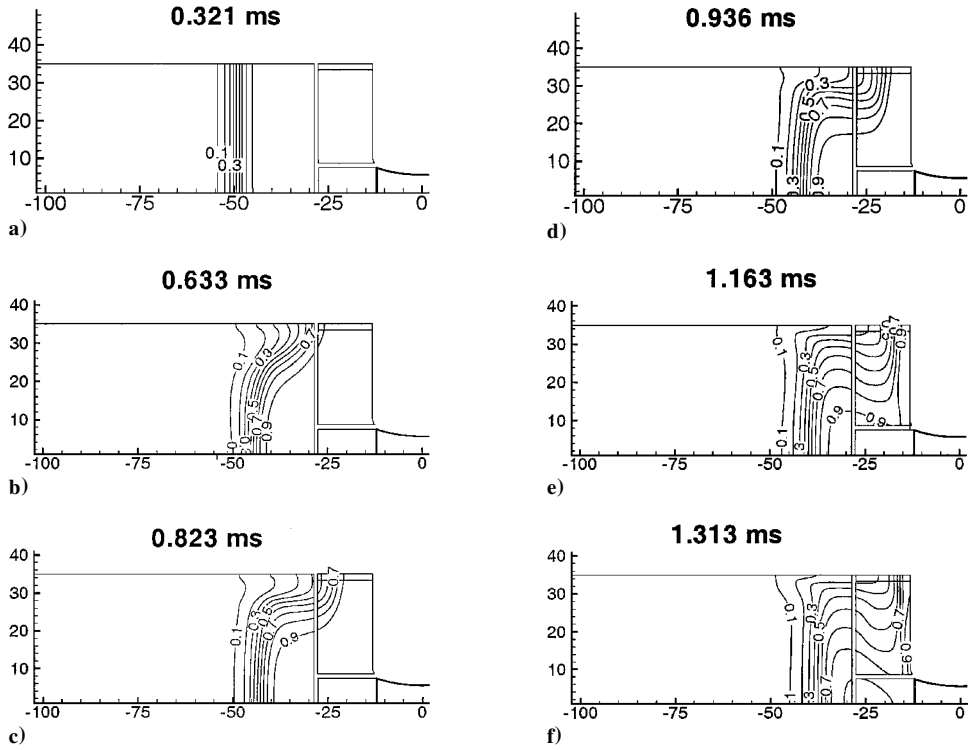

Fig. 3 N_2 mass fraction contours at different times in Euler computations.

diffusion effect of the numerical method for capturing the contact surface between the N_2 and He gases.

B. Navier–Stokes Solutions

In the Navier–Stokes (NS) computations, the initial solution plane is obtained after 0.272 ms from the diaphragm rupture. Figure 4 shows the evolution of the nondimensional density contours ρ/ρ_5 (ρ_5 is the density behind the reflected shock) at eight different times in only a part of the computational domain. On this initial plane, the density is almost constant behind the incident shock wave, except in the wall boundary layer (Fig. 4a). The thickness of the boundary layer is about 8×10^{-4} m. The shock wave reflects to the end of the tube, and its interaction with the boundary layer creates a bifurcated foot shock whose height increases with time (Figs. 4b and 4c). The establishment of the nozzle flow after the shock reflection can be also shown. From the numerical solution, before its interaction with the contact, the angle of the bifurcated foot measured relative to the tube wall is approximately equal to 37 deg (Figs. 4b and 4c). This value compares well with the theoretical value of 37.5 deg given by the Davies and Wilson model.[6] The reflected shock interacts with the contact surface at time 0.327 ms (Fig. 4d), and after this interaction, the He driver gas passes through the bifurcated foot and penetrates the test gas N_2 as a tongue (Fig. 4e). The thickness of this tongue increases (Figs. 4f and 4g). It begins to curl and rolls up to a growing vortex, due to the presence of the ended wall tube. Thus, the flow in the nozzle is quickly contaminated (Fig. 4h). Moreover, this vortex tends to move the contact surface back, and a large part of the hot flow is trapped (Fig. 4h) and cannot be used in experiments due to the earlier contamination by the cold gas of the nozzle flow.

To better understand this complex flow behavior, the velocity vectors are superimposed on the temperature contours at the same times in Figs. 5a–5h. The following effects, such as the bifurcated foot of the reflected shock near the wall and the creation of a reverse flow between the two oblique shocks and of a jet behind the second oblique shock, can be underlined again. Also note that, when the reflected shock interacts with the contact surface and moves back, the tailored contact surface near the wall is strongly deformed due to the presence of the jet, wherein its height and its velocity increase. This jet, having a tongue shape and composed of cold driver gas, pushes back the contact surface, curls, and rolls up to a main vortex before its entrance into the nozzle. The formation of this main vortex is accompanied by a small one at the corner of the tube with a contrarotative velocity.

Figure 6 shows, for time $t = 0.500$ ms after the diaphragm rupture, a more precise description of the flow between the Euler and Navier–Stokes computations, where the velocity vectors and the nondimensional density contours are drawn. In the inviscid flow (Fig. 6a), the velocity values are quasi null in most of the hot test gas, except near the nozzle entrance. The contact surface is slightly incurved near the wall due to the flow starting in the nozzle. Its position on the symmetry axis can be estimated between 3 and 3.5 cm from the end of the tube. Note that the position, given by an analytical solution in tailored conditions, is located at 3.4 cm. In the viscous flow (Fig. 6b), the structure of the flow is completely different except in the convergent nozzle, where the velocity vectors are similar to Euler case. The rollup effect, the two vortices, the moving back of the contact surface, and the contamination of the nozzle hot flow by the He cold driver gas are clearly visible. The arrival time of the contact surface in the nozzle (5% of the He mass concentration) relative to the reflection of the incident shock wave is equal to 0.215 ms, and corresponds approximately to 16% of the ideal drainage time and to 25% of the inviscid test time. In the same way, note that this arrival time from the diaphragm rupture located between high/low pressure chamber is 0.495 ms, which is close to 0.450 ms, a value given by the analytical approximation of Davies and Wilson.[6]

To deduce the useful test time that corresponds to the steady flow in the nozzle, the evolution of the nondimensionnal static pressure P/P_5 at the centerline just after the nozzle throat is plotted in Fig. 7. The first pressure peaks are due to the establishment of the steady nozzle flow. The last ones are produced by the He arrival.[9] Between these peaks, the pressure is quasi constant, and the useful test time can be evaluated at about 80 μs. Note that for approximately the same conditions, the measured useful test time by Chaix et al.[21] in the TCM2 facility is around 800 μs. Thus the ratio of the experimental/numerical useful test time is 10 and corresponds to the ratio of the exact/numerical shock tube length.

To study the grid refinement on the numerical solutions and more particularly on the reflected shock/boundary-layer interaction, the minimum y step $\Delta y_{\min} = 2 \times 10^{-5}$ m is multiplied and divided by a factor of two, respectively. The nondimensional static pressure P/P_2 distributions (P_2 is the pressure behind the incident shock), along

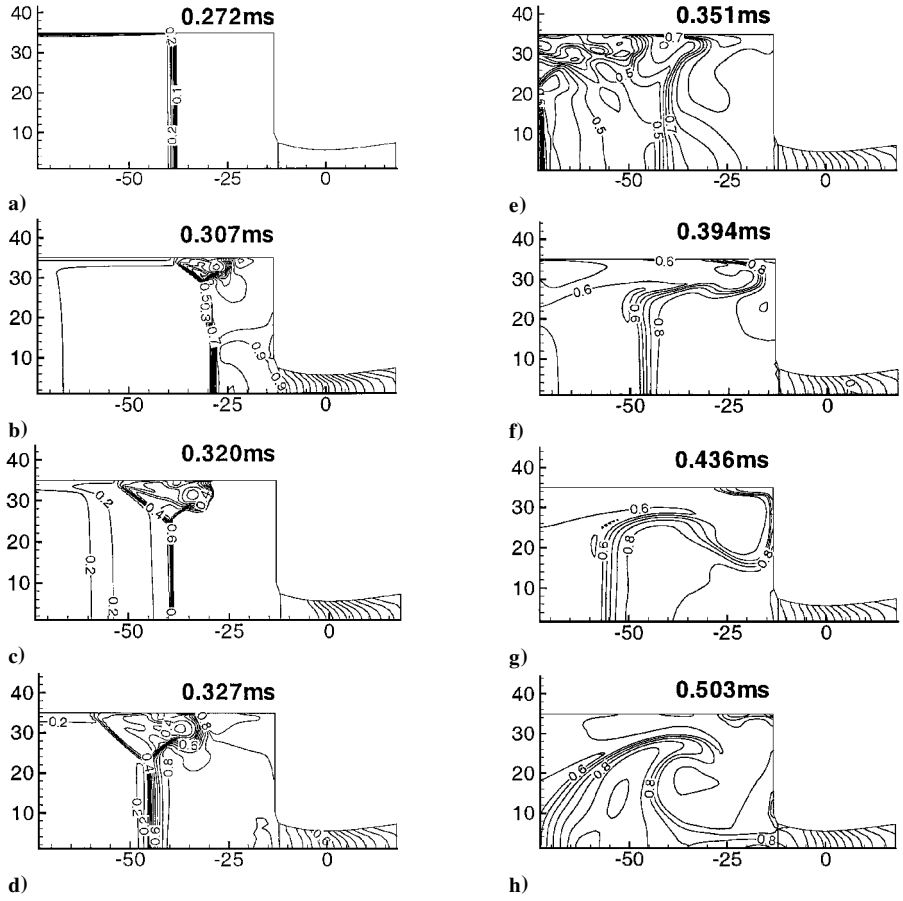

Fig. 4 Nondimensional density contours at different times in NS computations.

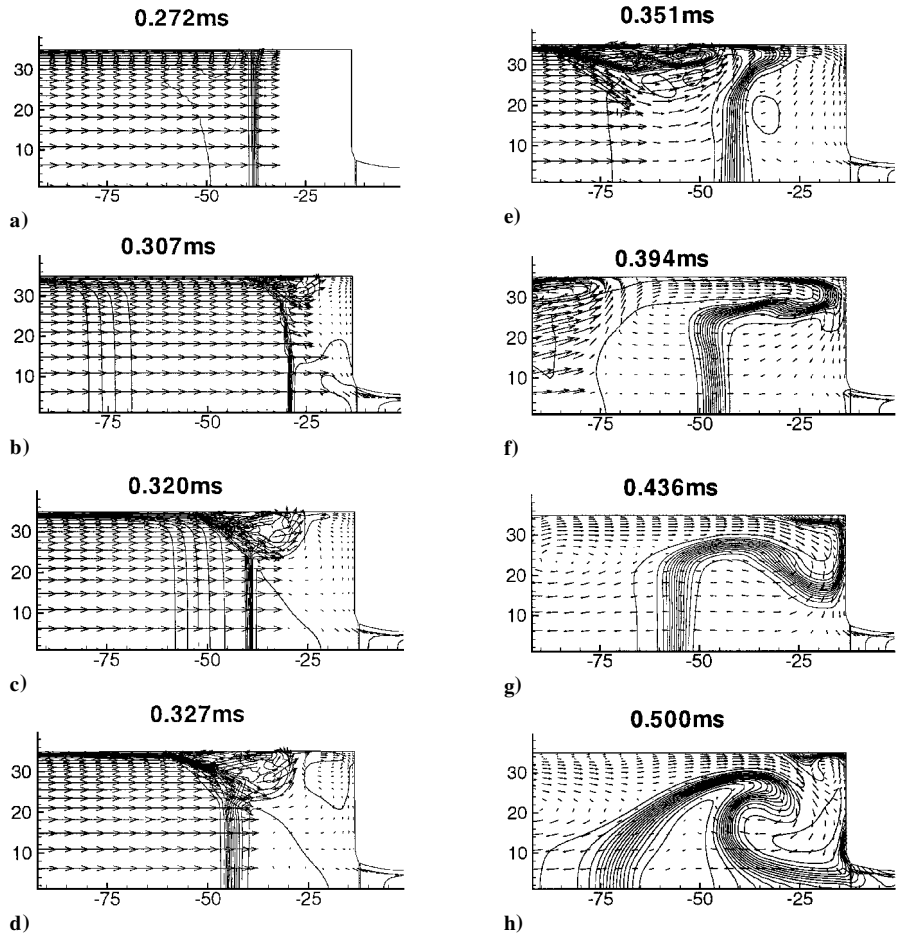

Fig. 5 Nondimensional temperature contours and velocity vectors at different times in NS computations.

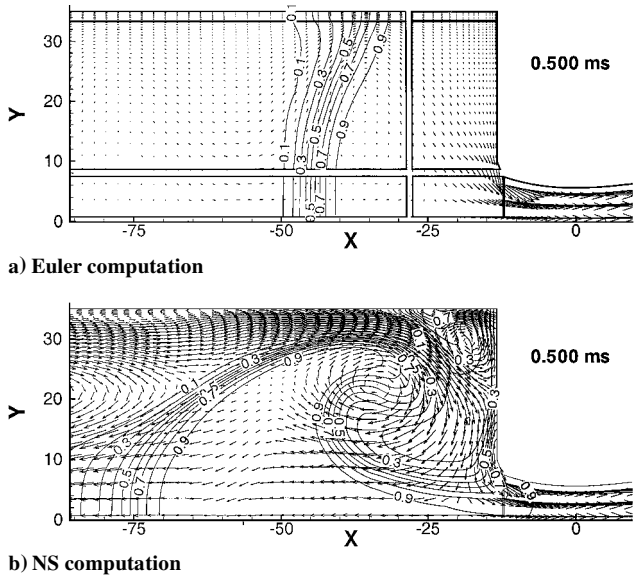

Fig. 6 Nondimensional density contours and velocity vectors at t = 0.500 ms after the diaphragm rupture.

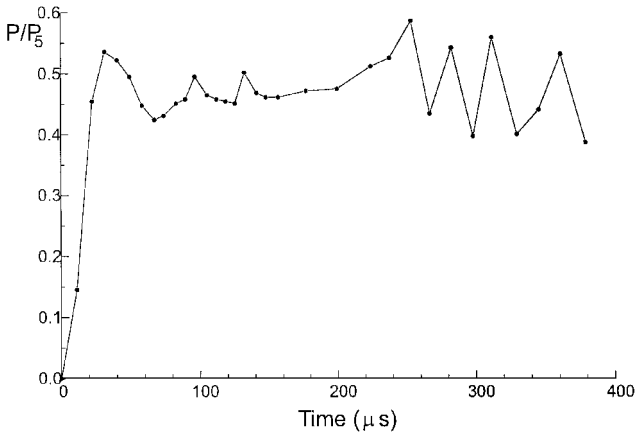

Fig. 7 Time evolution of the nondimensional static pressure just after the nozzle throat.

the shock tube wall and centerline, are plotted in Fig. 8. The pressure distributions obtained with $\Delta y_{\min} = 2 \times 10^{-5}$ m (reference solution) and $\Delta y_{\min} = 1 \times 10^{-5}$ m are quasi identical except for the slight shift of the shock position due to the influence of the spatial resolution on the time step.[22] These profiles contain the main features of the bifurcated flow, namely, the rise of the pressure through the front foot and at the rear of the interaction zone and the strong pressure gradients due to the unstable shear layer between them. The pressure profiles along the centerline are quasi identical for the three chosen steps. Note that the pressure values at the end wall of the shock tube are close to the theoretical one. It can be concluded that the reference solution contains all of the flowfield physics of the reflected shock wave/boundary-layer interactions.

C. Wall Suction Effect to Delay This Contamination Effect

As shown before, the premature driver gas contamination of the nozzle flow is mainly due to the jet formation near the wall and its growth behind the foot of the reflected shock. The tailored contact surface is trapped by this jet and rolls up in the hot flow region. When this effect is analyzed, it is obvious that a means of avoiding this contamination effect is to absorb this cold gas jet near the tube wall. However, the velocity of this jet may depend on the interface velocity after shock interaction (under-, over-, or tailored interface).

1. *Trapping by a Slit at the Corner*

Dumitrescu[14] proposed placing an absorbing slit at the corner of the end wall of the tube. This method was implemented in the multiblock code through a nozzle with a throat diameter of 1.8 mm. The nozzle flow through the slit starts just after the reflected shock.

The evolution of the N_2 mass fraction contours and the distribution of the velocity vectors at different times are shown in Fig. 9. The structure of the flowfield is the same as before, and the suction of the flow at the corner only avoids the formation of the small corner vortex, but not the main vortex. This the reason why the driver gas is not well captured and the contamination process is not delayed. The same result is obtained when the suction slit at the corner is located vertically.[17] This poor result was expected after analyzing the flowfield obtained first by NS computations. Recently, this conclusion was confirmed experimentally[15] and numerically.[16,17] Note also that different heights of the slit openning were tested experimentally by Chue and Dumitrescu,[16] who claim that the proposed suction devices do not produce a great effect on the flow of the driver gas. Now, it is evident that, to obtain a better effect, it is necessary to trap the jet as soon as it forms behind the reflected shock wave.[15,17]

2. *Trapping by a Slit Extended by a Sleeve*

A sleeve is added to extend the slit hole to cause suction before the end of the wall tube. The height of the gap between the sleeve and the shock tube wall was fixed at 1.8 mm. After different tests, which will not show here, the better suction effect is obtained with a sleeve length of 1.5 cm. This value corresponds to the distance between the end wall tube and the back of the recirculation zone behind the bifurcated foot of the reflected shock (Fig. 4e), when this shock interacts with the contact surface.

The evolution of the N_2 mass fraction contours and the distribution of the velocity vectors, at different times, are plotted in Figs. 10a–10f. Note the efficient early suction of the sidewall, which delays the recoil of the contact surface foot (Fig. 10d). However, the propagation of the He jet is not completely stopped, and the contact surface can be seen to roll up again (Fig. 10e). The latter causes the central part of this contact surface to move back and trap a small part of the hot test gas again (Fig. 10f). Nevertheless, the contamination of the nozzle flow is produced later. The 5% He contamination at the nozzle entrance can be observed at a time of 0.680 ms. If the shock arrival time at the end tube wall is substracted, the hot flow time is 0.400 ms. Thus, trapping by a sleeve delays the cold gas contamination and increases the useful time by a factor of 1.8.

Note that this device was very recently implemented in the T5 facility by Sudani et al.[15] and these authors claimed that "this device for capturing driver gas upstream yields a remarkable increase of the test time only for overtailored conditions. Nevertheless, the improved times are still shorter that the test time without device at slightly undertailored conditions. But the reservoir pressure constancy deteriorates markedly." Note also that the exact tailoring conditions in these experiments are not easy to know. Moreover, in high-enthalpy flows, this device may have some problems that need to be solved for practical use because of the strength of the sleeve for a high temperature and high pressure.[15]

3. *Trapping by a Conical Ring*

To improve this device, a new shape, presented in Fig. 11 and called a conical ring, is studied. In this device, the lower lip is slightly shifted downstream to have a diagonal opening section to improve the suction, which can be caused in horizontal and vertical directions. This conical ring is located in the same position as the sleeve. As before, several locations were tested. They lead to less efficiency of the contamination delay, and these results will not be presented in this paper.

The numerical results of this case are presented through the N_2 mass fraction contours and velocity vectors, for different times, in Figs. 12a–12f. In comparison with Fig. 10, the suction, along the wall and vertical to the main flow, reduces the main vortex formation and the moving back of the contact surface. This contact surface is first stopped and then moves upstream due to the suction and the hot nozzle flow. The global behavior of the reservoir hot flow seems to be closer to the Euler one. The 5% of the He mass concentration reaches the nozzle entrance at a time of 0.820 ms without trapping hot gas in the shock tube. The contamination effect is greatly delayed.

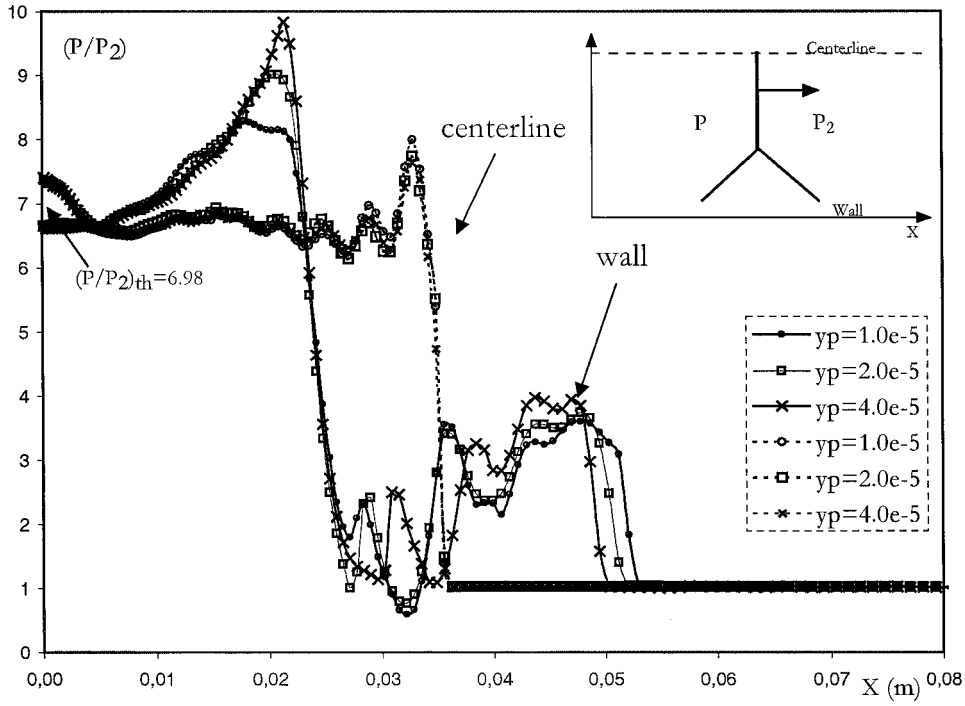

Fig. 8 Distribution of the nondimensional static pressure along the the centerline and the wall of shock tube.

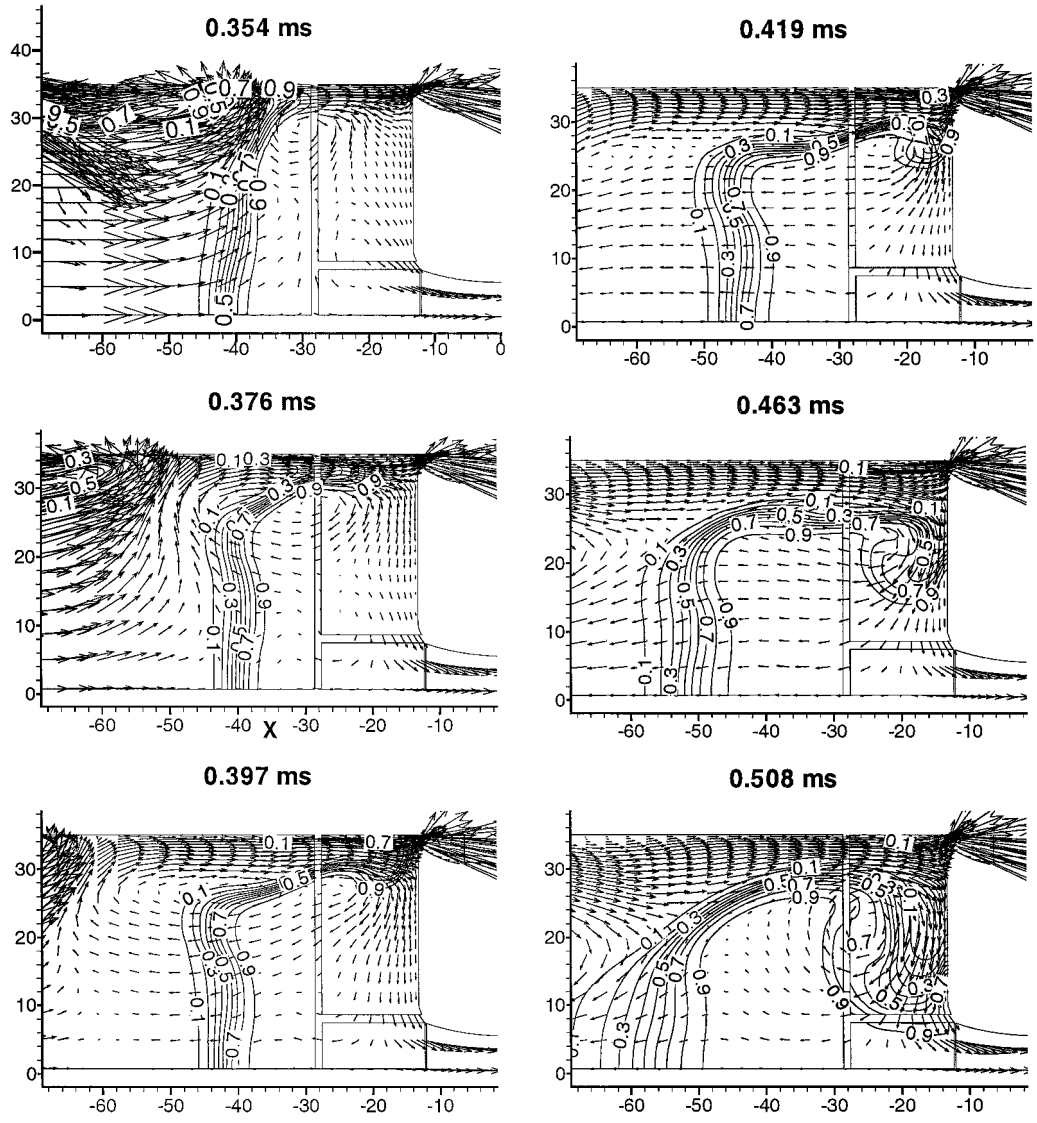

Fig. 9 N_2 mass fraction contours and velocity vectors at different times with suction by a corner slit.

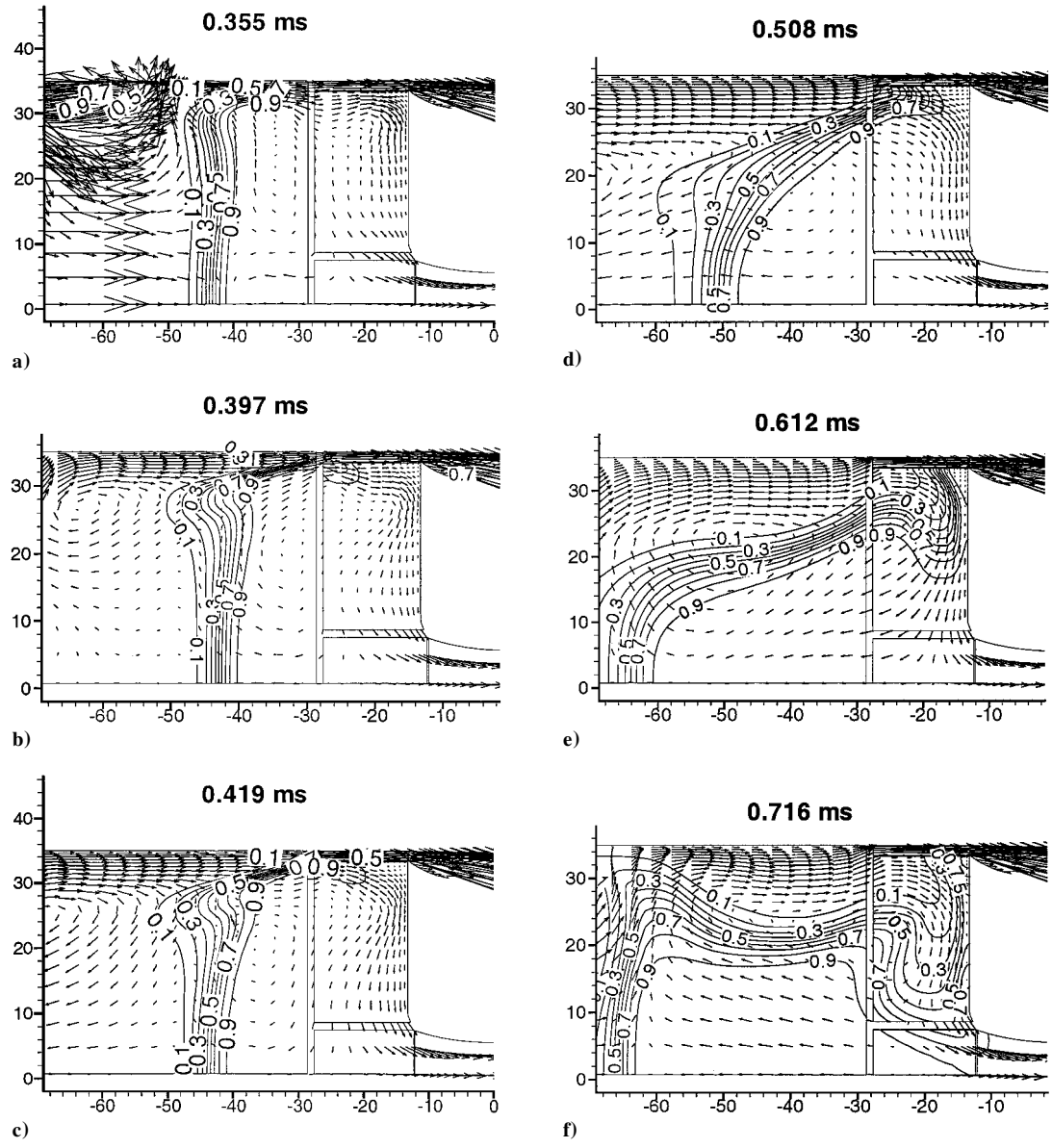

Fig. 10 N_2 mass fraction contours and velocity vectors at different times with suction by a corner slit extended by a sleeve.

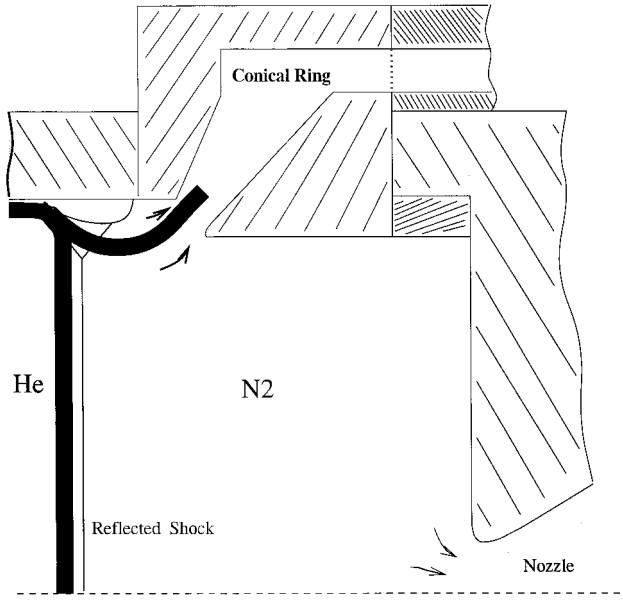

Fig. 11 Design of the conical ring.

To compare the driver gas contamination time in all presented cases, He mass fractions against time at the nozzle entrance is plotted in Fig. 13. The time origin is taken equal to 0.280 ms and corresponds to the shock arrival at the end wall of the tube. In Fig. 13, the horizontal line denotes 5% of the He mass concentration, and the arrival time of this He mass fraction is 0.215 ms in computations without a device, 0.400 ms with the sleeve, and 0.540 ms with the conical ring device. In this last case, the contamination is significantly delayed by a factor of 2.5 in comparison to the one without a device. At a distance of 2.3 mm after the nozzle throat and for each studied case, the nondimensional pressure evolutions P/P_5, where P_5 is the reservoir pressure, are plotted in Fig. 14 to evaluate the influence of the flow mass loss due to the suction effect. First without suction and in Euler computations, the pressure tends to a plateau with a value of 0.42, after some oscillations due to the unsteady nozzle starting flow. In NS computations, this average value is sigthly higher, due to the viscous effects. A more disturbed behavior and large peaks after 0.220 ms can be observed. With the suction devices, the average pressure is again around the Euler value, with less amplitude for the disturbances than without the device. It can be considered that an acceptable mass loss is due to the suction device. Finally, it can also be noted that trapping by a conical ring leads to less noisy pressure behavior and does not significantly affect the pressure level in the nozzle.

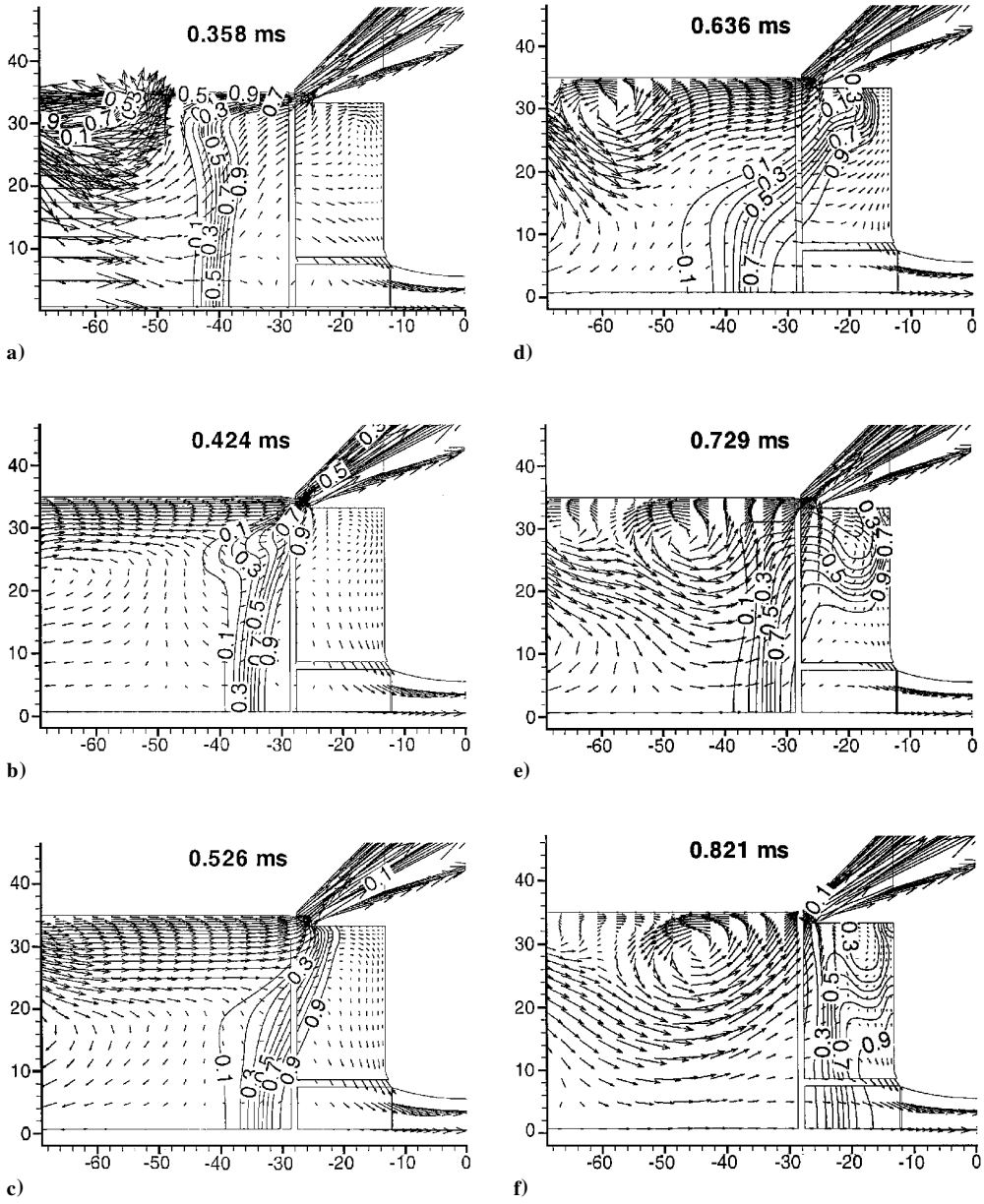

Fig. 12 N_2 mass fraction contours and velocity vectors at different times with suction by a conical ring.

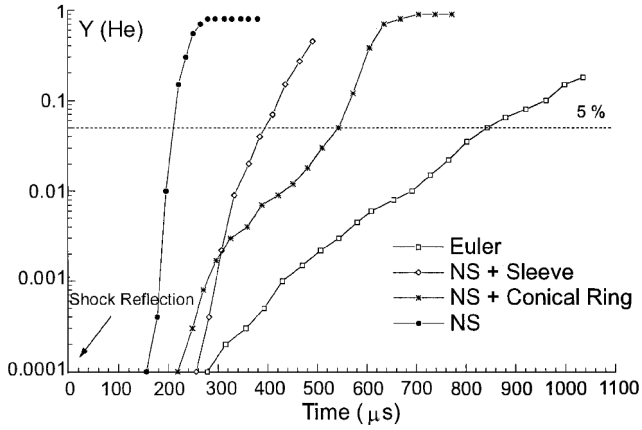

Fig. 13 Time evolution of He mass fractions at the entrance of the nozzle in the different cases.

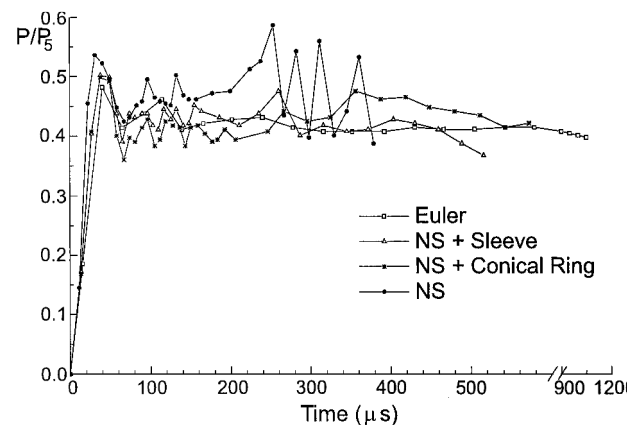

Fig. 14 Time evolution of nondimensional static pressure just after the nozzle throat in the different cases.

V. Conclusions

The unsteady viscous laminar flow in an impulse shock tunnel was described by solving the NS equations with the CARBUR code. These numerical simulations included the couple He/N_2 as driver/driven gases, the propagation of the incident shock wave and interface, the interaction of the reflected shock with the wall boundary layer, and the interface and the starting process in the hot nozzle flow. Under tailored conditions, the computations were conducted until the contamination of the nozzle flow by the cold driver gas, to describe it with accuracy and to better understand this phenomenon and to deduce the He arrival time. Different devices, based on the flow suction, have been studied to delay this contamination.

From the analysis of these numerical flowfields, a new device, a conical ring, is proposed, including a horizontal and vertical suction at the wall, to capture the driver gas jet upstream. In our case, this device is located at 1.5 cm before the end wall of the tube, but this location depends on the initial conditions (shock/interface interaction location) and geometrical dimensions of the tube and can be found numerically. In comparison to the computations for no device, the He arrival time in the nozzle is increased by a factor of 2.5. However, further numerical and experimental studies are needed to improve this device and to avoid the premature contamination in these hypervelocity shock tunnel facilities completely.

References

[1]Copper, J. A., Miller, H. R., and Hameetman, F. J., "Correlation of Uncontaminated Test Durations in Shock Tunnels," *Fourth Hypervelocity Techniques Symposium*, Arnold Engineering Development Center, Tullahoma, TN, 1965, pp. 274–310.

[2]Roshko, A.,"On Flow Duration in Low-Pressure Shock Tubes," *Physics of Fluids*, Vol. 3, 1960, pp. 835–842.

[3]Mirels, H., "Test Time in Low Pressure Shock Tubes," *Physics of Fluids*, Vol. 6, 1963, pp. 1201–1214.

[4]Zeitoun, D., and Imbert, M., "Interaction Between the Unsteady Boundary Layer and Inviscid Hot Flow in a Shock Tube," *AIAA Journal*, Vol. 17, No. 8, 1979, pp. 821–827.

[5]Mark, H., "The Interaction of a Reflected Shock with the Boundary Layer in a Shock Tube," NACA TM 1418, March 1958.

[6]Davies, L., and Wilson, J. L., "Influence of Reflected Shock and Boundary-Layer Interaction on Shock Tube Flows," *Physics of Fluids*, Supplement 1, 1969, pp. I-37–I-43.

[7]Stalker, R. J., and Crane, K. C. A., "Driver Gas Contamination in a High-Enthalpy Reflected Shock Tunnel," *AIAA Journal*, Vol. 16, No. 3, 1978, pp. 277–279.

[8]Nishida, M., and Lee, M. G., "Reflected-Shock/Side Boundary-Layer Interaction in Shock Tube," *Proceedings of the 20th International Symposium on Shock Waves*, Vol. 1, World Scientific, Singapore, 1996, pp. 705–710.

[9]Chue, R. S. M., and Itoh, K., "Influence of Reflected Shock/Boundary-Layer Interaction on Driver Gas Contamination in High-Enthalpy Shock Tunnels," *Proceedings of the 20th International Symposium on Shock Waves*, Vol. 1, World Scientific, Singapore, 1996, pp. 777–782.

[10]Wilson, G. J., Sharma, S. P., and Gillespie, W. D., "Time Dependent Simulations of Reflected Shock/Boundary-Layer Interaction," AIAA Paper 93-0480, Jan. 1993.

[11]Slade, J. C., Crane, K. C., and Stalker, R., "Driver Gas Detection by Quadrupole Mass Spectrometry in Shock Tunnels," *Proceeding of 19th International Symposium on Shock Waves*, Vol. 1, Springer-Verlag, Heidelberg, Germany, 1993, pp. 293–298.

[12]Paull, A., and King, M. D., "A Driver Gas Detection Device for Shock Tunnels," *Shock Waves*, Vol. 4, No. 5, 1995, pp. 289–291.

[13]Sudani, N., and Hornung, H. G., "Gasdynamic Detectors of Driver Gas Contamination in a High-Enthalpy Shock Tunnel," *AIAA Journal*, Vol. 36, No. 3, 1998, pp. 313–319.

[14]Dumitrescu, M. P., "Trapping the Boundary Layer: a Method to Diminish Flow Contamination in Shock Tunnels," *Proceedings of the 20th International Symposium on Shock Waves*, Vol. 2, World Scientific, Singapore, 1996, pp. 1581–1586.

[15]Sudani, N., Valiferdowsi, B., and Hornung, H. G., "Test Time Increase by Delaying Driver Gas Contamination for Reflected Shock Tunnels," AIAA Paper 98-2771, June 1998.

[16]Chue, R. S. M., and Dumitrescu, M. P., "Boundary-Layer Suction Device: Preliminary Investigations," *Proceedings of the 21st International Symposium on Shock Waves*, Vol. 1, Panther, Great Keppel, Australia, 1997, pp. 549–556.

[17]Cardoso, M., Burtschell, Y., Zeitoun, D., and Abgrall, R., "Numerical Simulation of Different Methods for Avoiding Driver Gas Contamination in Shock Tunnels," *Proceedings of the 21st International Symposium on Shock Waves*, Vol. 1, Panther, Great Keppel, Australia, 1997, pp. 537–542.

[18]Cardoso, M., "Contribution Numerique à l'Etude des Ecoulements à Haute Enthalpie," Ph.D. Dissertation, Dept. Milieux hors d'Equilibre, Univ. de Provence, Marseille, France, Sept. 1997.

[19]Burtschell, Y., Brun, R., and Zeitoun, D., "Two-Dimensional Numerical Simulation of the Marseille University Free-Piston Shock Tunnel TCM2," *Proceedings of the 18th International Symposium on Shock Waves*, Vol. 1, Springer-Verlag, Heidelberg, Germany, 1991, pp. 583–590.

[20]Flandrin, L., Charrier, P., and Dubrocca, B., "A Robust Finite Volume Method for Computations on Two-Dimensional Unstructured Hybrid Meshes," *Computational Fluid Dynamics '94*, Wiley, Chichester, England, U. K., 1994, pp. 301–308.

[21]Chaix, A., Dumitrescu, M. P., Dumitrescu, L. Z., and Brun, R., "Calibration of the TCM2 Conical Nozzle and Internal Flow Investigations," *Proceedings of the 21st International Symposium on Shock Waves*, Vol. 1, Panther, Great Keppel, Australia, 1997, pp. 1151–1156.

[22]Weber, Y. S., Anderson, J. D., Oran, E. D., and Boris, J. P. "The Numerical Simulation of Shock Bifurcation Near the End Wall in a Shock Tube," AIAA Paper 94-2307, June 1994.

M. Sichel
Associate Editor